Damage evolution in freeze cast metal/ceramic composites exhibiting lamellar microstructures

C. Simpson, P.J. Withers
School of Materials, University of Manchester, M13 9PL
Research Complex at Harwell, Rutherford Appleton Laboratory, OX11 0FA
christopher.simpson@manchester.ac.uk

T. Lowe
School of Materials, University of Manchester, M13 9PL

S. Roy, A. Wanner
Institut für Werkstoffkunde I, Karlsruher Institut für Technologie, 76128 Karlsruhe, Germany

ABSTRACT. The damage evolution in a single domain aluminium/alumina freeze-cast composite has been examined using 3D X-ray computed tomography (CT). A single domain was extracted and loaded incrementally at an orientation of 45° to the lamellae, with the damage being assessed after each of eight compressive loading steps. Prior to loading, significant damage was observed at the metal-ceramic interface – this is thought to have formed during machining and can be ascribed to weak interfacial bonding associated with the Cu coating applied to the ceramic preform prior to metal infiltration. Further interfacial damage was seen to initiate after loading to 170MPa and to develop with each subsequent load step. Damage was also observed in the ceramic lamellae, with a series of parallel cracks forming across the alumina, perpendicular to the domain orientation. These sets of parallel, intra-lamellae cracks were closely spaced, but initiated independently, with coalescence only occurring at higher loads. Both the interfacial and intra-lamellae cracking initiated after loading to 170MPa, with the intra-lamellae cracks propagating into the metal matrix after loading to 240MPa. The cracks in the ceramic lamellae were found to form and develop independent of the interfacial cracks, with discrete crack paths and morphologies being observed in each case. Despite this, the underlying driving force was the same for each damage mode, with crack propagation being driven by an elastic-plastic mismatch between the metal matrix and ceramic lamellae.

KEYWORDS. Crack growth; Time-lapse CT; MMC; Computed tomography.

INTRODUCTION

Over the past three decades metal matrix composites (MMCs) have progressed from being a topic of academic interest to one of practical importance, with MMCs finding usage in automotive and aerospace applications [1]. Their rapid adoption has been due their attractive mechanical properties, which include high strength-to-weight ratios, stiffness and wear resistance. More recently there has been an impressive diversification in MMC manufacturing

technology, with advances being made in terms of both composition and processing techniques [2]. One of the more promising processing techniques is that of ice-templating, which is also known as freeze-casting. This process revolves around the formation of a second phase scaffold via segregation [3]. The second phase is suspended or dissolved into a solvent before being rejected ahead of the advancing solidification front during cooling. This solvent can then be removed via sublimation, leaving the underlying green body. In the case of an MMC, this unsintered template would comprise of ceramic particles, which would be sintered and densified prior to being infiltrated with the metallic matrix. The versatility of this approach is noteworthy, with a modification of the freeze temperature and solvent supersaturation allowing for a vast array of template morphologies [3]. In the MMC of interest to this study, the freeze methodology has been chosen (and refined) to allow for the precisely controlled formation of a multi-domain lamellar with a consistent and optimised lamellae spacing [4]. An example of the resultant microstructure can be seen in Fig. 1. The microstructure of an individual domain is better shown in Fig. 2.

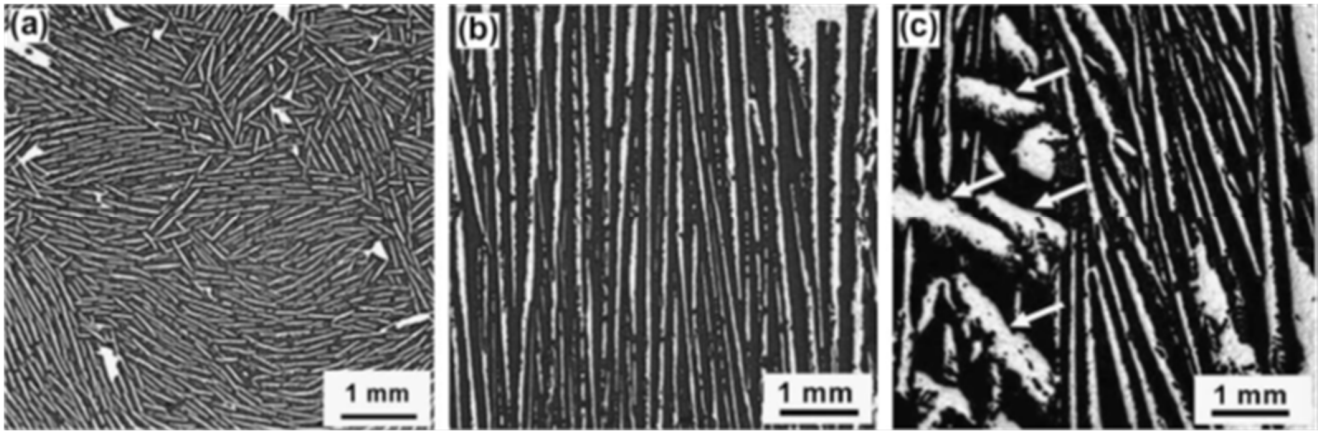

Figure 1: Typical lamellar microstructure of a multi-domain composite at three different orientations: (a) face orientated perpendicular to the freezing direction and (b and c) faces orientated parallel to the freeze direction. Samples are extracted from the individual domains seen in (a), with the orientation, α, corresponding to the orientation of the lamellae as seen in this image [5].

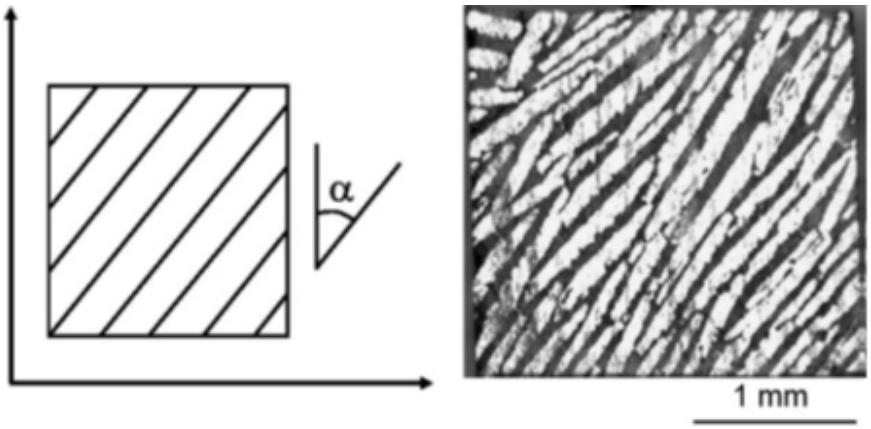

Figure 2: Typical lamellar microstructure of a single domain sample with a domain orientation of α=45° [5].

The domain level integrity of these composites has been studied by Roy et al [5], [6]. This work highlighted the anisotropic response of individual domains of freeze-cast lamellar composites, with the strength being well described by the energy-based Tsai-Hill criterion [7], expressed as:

$$\frac{1}{\sigma_x^2} = \frac{\cos^4\alpha}{X^2} + \left(\frac{1}{\tau_{LT}^2} - \frac{1}{X^2}\right)\sin^2\alpha\,\cos^2\alpha + \frac{\sin^4\alpha}{Y^2}. \quad (1)$$

The compressive strength longitudinal and perpendicular to the freeze cast direction (i.e. α = 0° and 90°) are denoted by X and Y respectively and the composite shear yield, τ, is based on the shear yield of the metal matrix. The orientation specific compressive strength of the composite is given by σ_x and is associated with a domain orientation α. The minimum

compressive strength and maximum strain to failure were observed at an angle of 45°, which corresponds to a failure mechanism controlled by the shear yield behaviour of the metal. Bridging of the ceramic preform across the metallic lamellae [8] does, however, act to strengthen the composite in this orientation [5]. Although the interface between the aluminium and alumina has been shown to be strong [5, 9], there is still an interest in investigating and potentially exploiting new coatings on the preform with the aim of further improving the strength or toughness of the composite. Initial work by Roy et al. [5] suggests that the strength of the interface and ultimately of the bulk composite decreases upon the application of a Cu coating to the preform. This is ascribed to the formation of a CuO_2 layer during processing, which weakens the interface and inhibits the dissolution of Cu into the aluminium matrix.
The study on domain orientation specific strength was complemented by an SEM examination of the damage progression with increasing load ($\alpha = 45°$) [5]. The authors were able to make some initial insights into the extent of the cracking and crack path but were limited by a 2D analysis of an inherently 3D problem. Techniques such as computed tomography (CT) are well suited to this type of work as they offer researchers the opportunity to more clearly identify crack initiation behaviour, whilst also monitoring the crack path, interconnectivity and the full extent of the damage with increasing load. The aim of this work is therefore to employ 3D CT to build on the initial analysis completed by Roy et al. [5, 6], with the aim of better understanding damage evolution at the domain level in freeze-cast lamellar composites.

MATERIAL PREPARATION

Alumina preforms were produced at the Institut fur Keramik im Maschinenbau (IKM) at the University of Karlsruhe via the freeze-casting of a ceramic suspension at -10°C. Water was used as the freeze-casting solvent with 0.5 wt. % Dolapix CE64 as a dispersant and 10 wt. % Optapix PAF60 as a binder. This solution contained 22 vol. % ceramic powder (CT3000SG from Almatis GmbH, Germany) with a nominal alumina content of 99.8 % and a particulate size of 2.5 µm. After freeze-drying for 48 h the preforms were sintered at 1550°C for 1h before being cooled to room temperature at 4°C min^{-1}. The preforms were then coated with Cu prior to infiltration with a eutectic aluminium-silicon alloy (Al-12Si). The infiltration was completed via squeeze-casting, with the preform being heated to 800°C prior to casting. After infiltration the composite was cooled to 450°C and held for 2h prior to a furnace cool. The resultant microstructure is that of a multi-domain composite, with a domain structure that consists of ceramic and metallic lamellae that run parallel to the freezing direction. Individual domains had a width in the order of 1-3 mm. From suitably sized domains cubic samples were extracted with a domain orientation, α, of 45° and a size of approximately 2.3 mm x 2.3 mm x 2.3 mm. Further details about the preparation of the preforms and final microstructure can be found in the work of Roy et al. [5] and Waschkies et al [4].

EXPERIMENTAL METHOD

To study the damage progression in the freeze-cast composite, an ex-situ 3D computed tomography experiment was carried out on a single domain sample having a lamellae angle of $\alpha = 45°$ (see Fig. 2). This work is a natural extension of the SEM work previously carried out by Roy et al [5]. The compressive loading was completed on a screw-driven Instron 3344, with the associated ex-situ imaging being undertaken after incremental loading up to a maximum compressive load of 1450 N. The load increments represent compressive stresses of 0 MPa, 65 MPa, 100 MPa, 135 MPa, 170 MPa, 205 MPa, 240 MPa and 275 MPa.
High resolution 3D analysis of these single domain composite samples was conducted using a Zeiss Xradia Versa 520 X-ray microscopy system based at the Henry Moseley Manchester X-ray Imaging Facility (HMXIF). The system was operated at 40 kV and a power of 3W, with a specimen to source and source to detector distance of 12 mm and 8 mm respectively. The sample was imaged using a 4x optical magnification giving a voxel size of 2.1 µm. The sample was rotated through 360°, with 1,601 projections being acquired utilising an exposure time of 10 s, resulting in a total scan time of approximately 5h. This data was reconstructed using the Zeiss proprietary XRM Reconstructor software using a filtered back projection algorithm. The post-processing and image analysis was carried out using Avizo 3D visualisation software (version 8.1). The resultant reconstructed volumes were characterised by a bright metallic matrix and darker ceramic lamellae. Although it is possible to distinguish between these phases, the limited attenuation contrast precludes any automatic or semi-automatic segmentation of the individual lamellae. Manual segmentation is possible and would be beneficial but the low attenuation contrast makes this very difficult and time consuming; the advantages of this approach were therefore not deemed to outweigh the practical constraints.

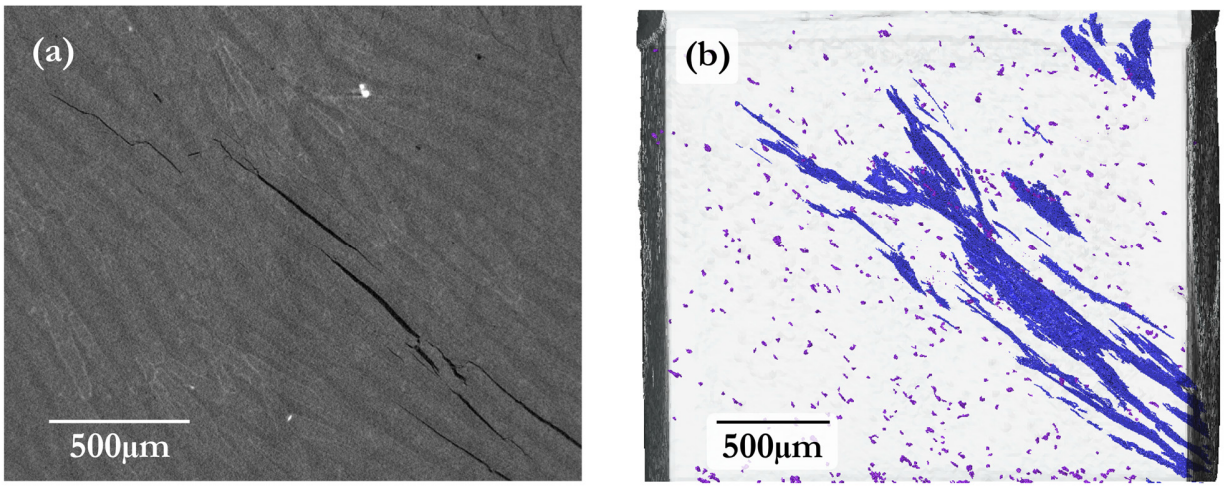

Figure 3: Initial state of sample prior to loading: (a) virtual 2D cross-sectional slice, showing the lighter aluminium matrix and darker alumina lamellae, (b) the associated, 3D segmented volume – it was not feasible to (automatically) segment the metal-matrix lamellae. The blue regions highlight the initial, pre-existing cracking while the purple highlights the porosity.

DAMAGE DEVELOPMENT

The sample was scanned and assessed prior to loading. Considerable damage was observed in the unstressed condition. This damage was seen to run along the interface between the metal and ceramic and was localised to a strip running centrally from the bottom right corner to the top left corner (i.e. at an angle of 45°). A 2D virtual slice of the lamellar microstructure showing the pre-existing damage can be seen alongside the associated, partially segmented 3D volume in Fig. 3. The segmented volume also highlights the porosity found in the sample.

The sample was then x-ray imaged and visualised after each of the incremental load steps, with the associated progression of cracking and damage highlighted in Fig. 4 for a central region of interest. No further damage was introduced upon increasing the loading to 135 MPa although the main pre-existing crack did close somewhat. Additional damage became apparent upon loading to 170 MPa with interfacial cracking occurring at some metal-ceramic interfaces and a small number of cracks arising in the alumina lamellae. The cracking in the alumina ran perpendicular to the lamellae orientation. These cracks are highlighted in Fig. 4c. Much of the damage created in this and subsequent load steps was localised to the central strip of material running parallel to the lamellae from the top left corner to the bottom right corner of the sample (see Fig. 3).

Increasing the load to 205 MPa increased the size of the cracks but did not appear to increase the number of cracks in this virtual slice. A more thorough investigation of the 3D volume highlighted a small increase in the number density of interfacial cracks and cracks in the alumina. At this stage the cracks in the alumina do not appear to be related to, or to initiate from, cracks formed at the metal-ceramic interface (or visa-versa). The two damage processes seem to be occurring separately and simultaneously. This question is revisited in the following section and is depicted (in 3D) in Fig. 5 and Fig. 6.

After increasing the load to 240 MPa the size and occurrence of cracked material have increased significantly, with numerous cracks being observed in the ceramic lamellae. The interfacial crack first highlighted at 170 MPa had extended and opened after this loading step. The final loading step (to 275 MPa) just prior to catastrophic damage, was accompanied by extensive cracking appearing both along the metal-ceramic interface and across the alumina lamellae. At this and the previous load of 240 MPa the cracks were able to penetrate from the ceramic lamellae into the metal matrix. This damage is difficult to resolve but can be seen in in Fig. 4f. Although cracks are propagating into the matrix there is no evidence of plasticity or necking in the metal surrounding these cracks. An additional load step (to 310 MPa) was attempted, and while the application of the load was successful, removal of the composite from the Instron 3344 testing machine resulted in sample failure. The composite had fractured along the previously described central damage zone and no further imaging of the sample was possible.

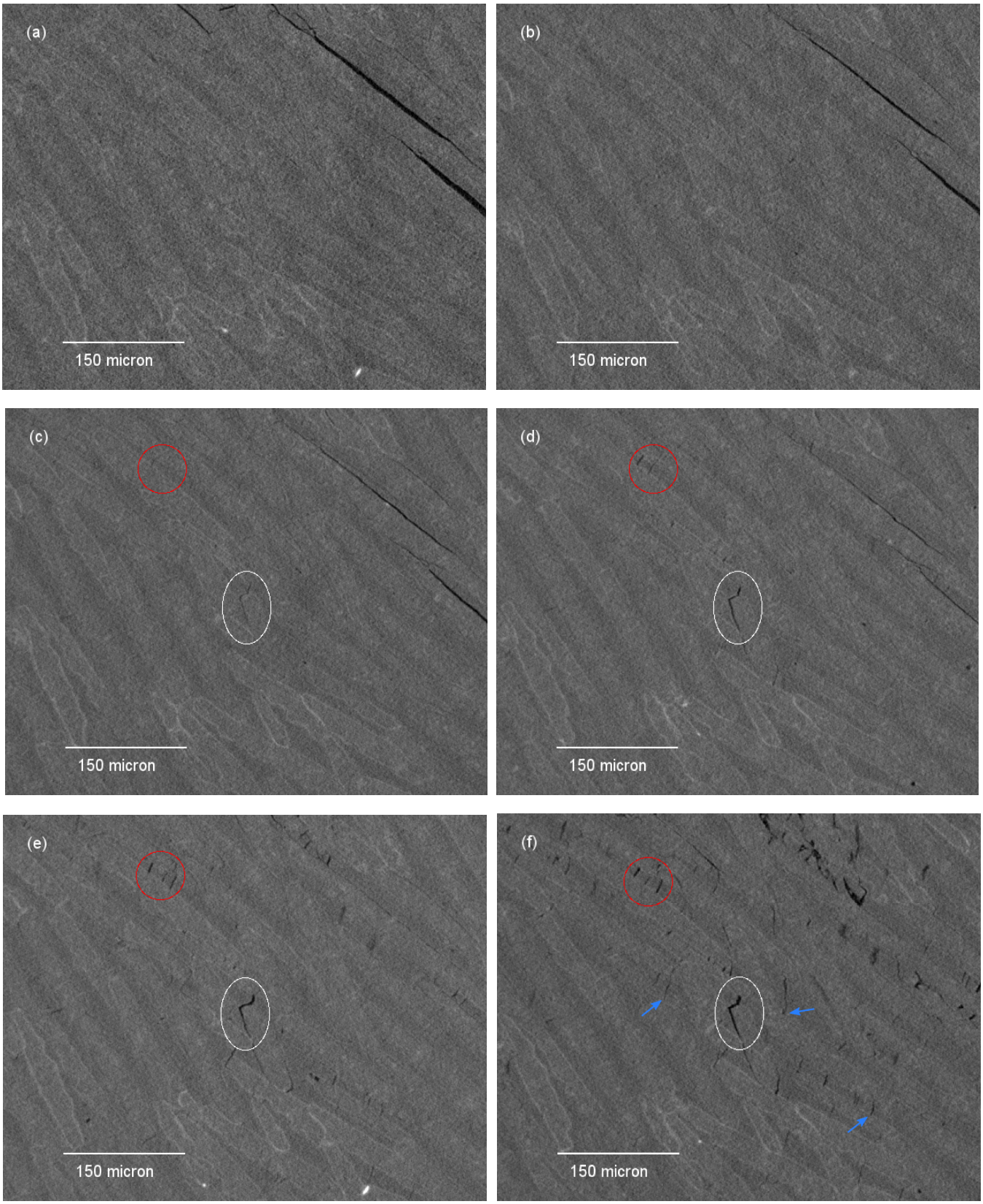

Figure 4: Damage evolution tracked for a central region of interest in one 2D slice (a) 0 MPa, (b) 135 MPa, (c) 170 MPa, (d) 205 MPa, (e) 240 MPa and (f) 275 MPa. Load applied vertically. The white circles correspond to the development of an interfacial crack, the red circles highlight the formation and growth of a series of intra-lamellae cracks and the blue arrows indicate cracking in the metal matrix.

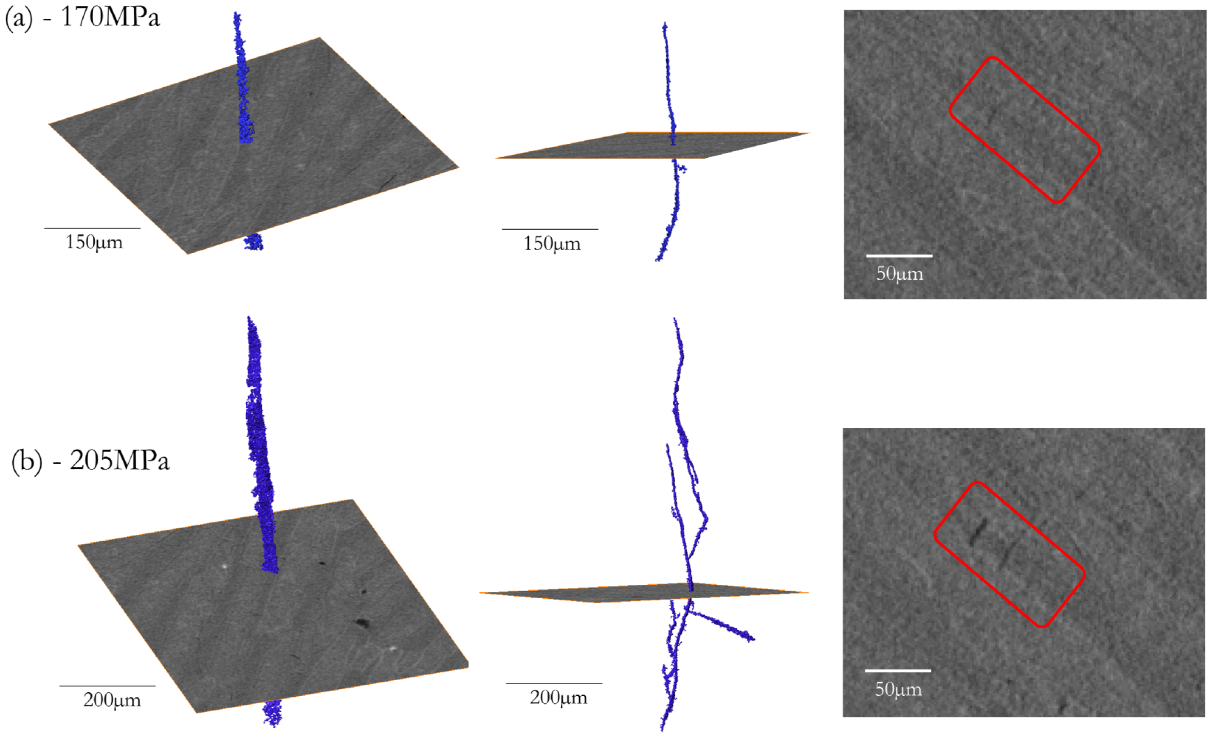

Figure 5: 2D/3D representation of the extent and development of a crack within a ceramic lamella after loading to (a) 170 MPa and (b) 205 MPa. The tracked damage corresponds to the feature circled in red in Fig. 4. The damage is predominantly constrained to a narrow band running across the alumina lamellae. Loading to 205MPa is seen to have caused a coalescence of two parallel cracks.

CRACK INITIATION AND TRACKING IN 3D

The initial sequence of 2D slices shown in Fig. 4 gives a broad overview of damage initiation and growth – an advantage of a 3D imaging system is that specific features and their path and interconnectivity can be tracked in a more complete, representative fashion. In this case, both the interfacial damage and intra-lamellae damage circled in Fig. 4 have been segmented and tracked from initiation through to the final loading step and sample failure. The progression of this damage is best demonstrated through an illustration of the cracks formed during loading to 170 MPa and 205 MPa, i.e. the loads steps in which damage was first observed. To this end, Fig. 5 highlights damage in the ceramic lamellae and Fig. 6 tracks crack formation at the metal-ceramic interface. It is important to stress that these cracks were not connected to the pre-existing damage until the final loading step (275 MPa). The two distinct types of damage are covered in the following sections.

Intra-lamellae cracking

Loading the sample to 170 MPa initiated a long, narrow intra-lamellae crack with a size of 50 µm x 500 µm (see Fig. 5). The 50 µm width corresponds to the thickness of the alumina lamellae that the crack propagated through. The crack ran perpendicular to the lamellae across its full length, with no significant deviation in orientation. The intra-lamellae crack did not interact with interfacial cracks and was not seen to deviate across the interface at this load. The segmented intra-lamellae crack adjoins 2 further cracks which run parallel within the same ceramic lamellae. These cracks have formed independent of one another, with no evidence of a common initiation point.

The intra-lamellae crack propagated after loading to 205 MPa, with the crack length increasing to 750 µm. The width of the crack was still largely constrained by the thickness of the alumina lamellae. The cracks running parallel to main, segmented intra-lamellae crack are more distinct at 205MPa and are seen to have joined with the primary crack. It is worth reiterating that these cracks did not have a common initiation site and that the observed mechanism is one of crack coalescence rather than crack branching. At this load the intra-lamellae crack was also found to propagate along select regions of metal-ceramic interface. The crack was not sharply deviating but rather propagating along regions of interface that were

aligned with the crack orientation (i.e. the end of a ceramic plate). Once the crack was running along the interface it was able to follow the boundary orientation and deviate away from the main crack. The extent of this branching is minimal (<50 μm) when compared to the scale and length of the main intra-lamellae crack.

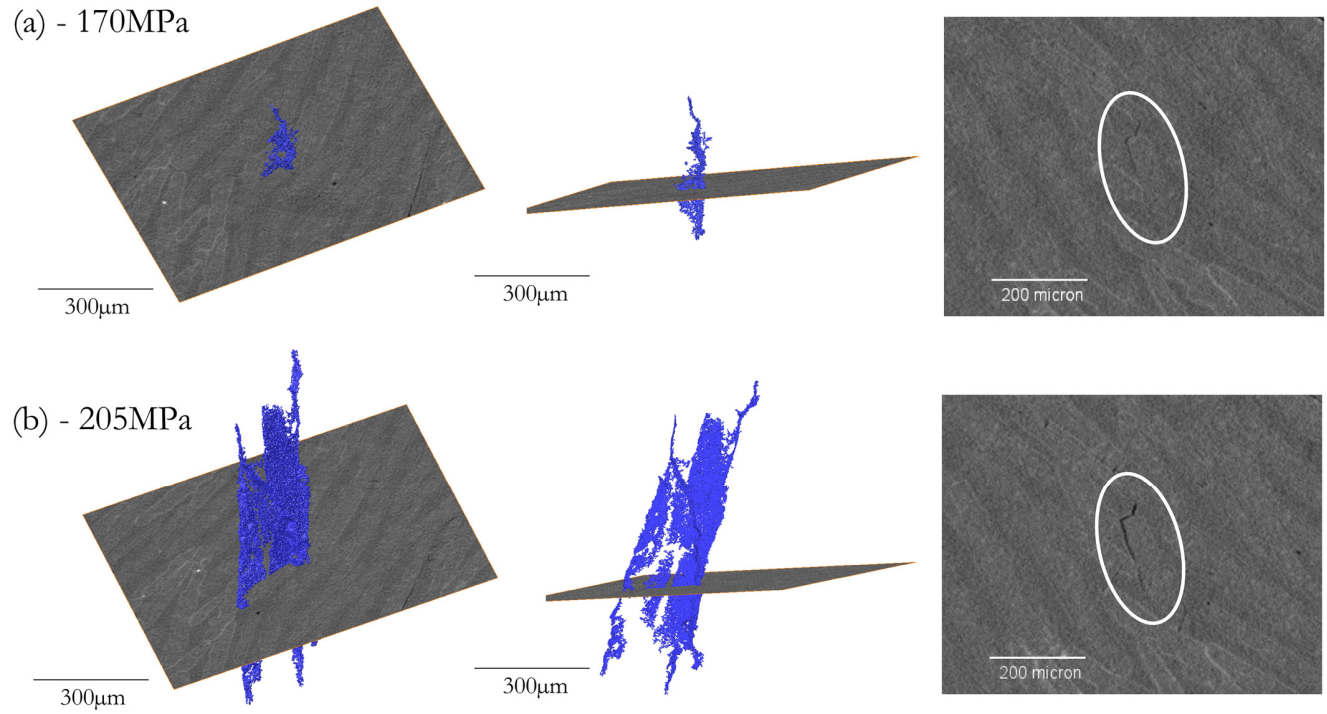

Figure 6: 2D/3D representation of the extent and development of a crack at the metal-ceramic interface after loading to (a) 170MPa and (b) 205MPa. The tracked damage corresponds to the feature circled in white in Fig. 4.

Upon loading to 240MPa there was further crack extension (>1mm) and more interaction with interfacial material and other, newly formed cracks. The crack was still predominantly constrained by the thickness of the ceramic lamellae, although there were regions in which the crack had extended into the metal matrix, thereby marginally increasing the width of the crack. As noted in the previous section, the damage and cracking observed at 275MPa was considerable, with the pre-existing cracking and freshly initiated damage coalescing. The tracked features were not assessed in detail at this point as it was not possible to differentiate between damage that could be ascribed to the cracking present prior to testing and that which initiated and propagated during testing.

Interfacial cracking

As was previously noted, interfacial damage also initiated upon loading to 170MPa. After this loading cycle the size of the tracked feature was approximately 150μm x 300μm, with the initiation point appearing to centre on a discontinuity in the metal-ceramic lamellae, such that the interface no longer ran at 45° (see Fig. 6a). At this load, there was no suggestion that the cracking was linked to damage originating in the ceramic lamellae. This is consistent with the findings presented in the previous section, in which cracks in the alumina were seen to form and progress without the assistance of cracking at the metal-ceramic interface. This supports the idea that the two damage modes are able to occur simultaneously but separately.

Increasing the load to 205MPa caused the tracked interfacial feature to increase in size to approximately 600μm x 300μm. The damage is wrapped around and growing along the interface of a truncated ceramic lamella. It is clear at this point, and after the subsequent load increments, that the size of the tracked and segmented interfacial crack is larger than that suggested on the corresponding 2D virtual slice; this phenomenon can be seen in Fig. 6b.

Upon increasing the load to 240MPa the interfacial damage propagated across the remainder of the sample and broke through the sample surface. The tracked interfacial damage also began to interact with other cracks, notably merging with intra-lamellae cracks and propagating across ceramic lamellae with greater frequency. The crack was significantly

anisotropic at this stage, with crack growth preferentially occurring perpendicular to the orientation of the images shown in Fig. 4 (in accordance with the orientation shown in Fig. 6).

DISCUSSION

A number of samples were tested from this batch of material and all had similarly extensive damage prior to loading. The weak interface associated with a Cu coated preform is the most likely explanation behind the damage. The Cu coating has been shown to weaken the interface between the metal and ceramic lamellae when compared to the inherently strong bond found between the alumina and aluminium [5]. This coating would therefore facilitate interfacial cracking during solidification or machining. Given that the damage appears to be sample specific (i.e. localised to a sample specific region of weakness), it seems likely that in our case the damage was induced during machining.

The 2D/3D CT assessment of the damage initiation and accumulation with increasing compressive load has highlighted the formation of cracks at the metal-ceramic interface and across the ceramic lamellae. The cracking in the ceramic lamellae, and lack of damage in the metallic matrix (at lower loads), are findings consistent with previous work by Roy et al [5]. The cracking in the ceramic is due to an elastic-plastic mismatch between the brittle ceramic and the ductile metal matrix. Plastic flow in the metal cannot be accommodated by the ceramic lamellae, which therefore fail. This leads to the formation of sets of parallel cracks, which relieve the interfacial stress; these cracks are closely spaced but separate, with no common initiation site being observed. The intra-lamellae cracks are able to propagate from the ceramic into the metal matrix at higher loads – these cracks would be expected to develop further with additional load steps but were not able to do so due to premature final failure occurring along the metal-ceramic interfaces. The cracks that are developing in the metal matrix do not appear to be associated with extensive local plasticity and necking although the resolution of the images and the size of these cracks would make this type of feature difficult to resolve.

The damage that was initiating along the metal-ceramic boundary can also be related to the weakened Cu coated interface. To elaborate on this point, the deformation at 45° is controlled by shear yielding through the softer metal matrix. This produces the noted elastic-plastic mismatch (and damage in the ceramic lamellae), which when coupled with a weakened interface, will also lead to the initiation and growth of interfacial cracks. Given that the underlying damage mechanism (i.e. elastic-plastic mismatch) is the same for both interfacial and intra-lamellae cracks, it is perhaps unsurprising that there is interaction and convergence between these damage types at high loads. What is, however, interesting is that the two damage modes are distinct, with each type of crack having been shown to initiate separately and propagate without significant divergence or interaction.

One final point to note is that the damage observed in the virtual 2D slices was not representative of the bulk 3D sample. The increase in crack length at the metal-ceramic interface with increasing load appeared minimal in the 2D slice. A full 3D analysis highlighted extensive anisotropic interfacial cracking, which was not obvious from the 2D slice and would not be apparent using an inherently 2D analysis technique such as SEM. This type of 3D approach is particularly beneficial in situations such as this and has allowed for a much clearer understanding of the damage progression and connection (or lack thereof) between the different cracks.

CONCLUSIONS

- The dominant failure mechanism is that of interfacial cracking at the boundary of the metal-ceramic lamellae. The damage accumulates at these regions due to an elastic-plastic mismatch between the metal and ceramic, which is accompanied by an interface weakened by the application of a Cu coating on the preform.
- Cracking is also observed within the ceramic lamellae; these cracks form transverse to the lamellae orientation and also result from the metal-ceramic elastic-plastic mismatch, which predominates at a lamellae orientation of α=45°. Sets of separate parallel cracks are initiated, which relieves the associated build up in stress. Cracking in the metal matrix is only seen at the maximum loads, just prior to failure and is limited by the extensive interfacial cracking and associated failure.
- The cracks in the ceramic lamellae and those at the metal-ceramic interface are initiating at the same load, namely 170MPa. They are, however, distinct from one another, with the crack morphologies, paths and lack of interaction differentiating them.

- Computed tomography has been shown to be a useful technique with which to monitor and describe crack initiation and growth in freeze-cast MMCs. This technique will be increasingly successful in complex systems such as multi-domain composites, where the crack path is likely to be more convoluted.

REFERENCES

[1] Clyne, T. W., Withers, P. J., An Introduction to Metal Matrix Composites. Cambridge University Press, (1993).
[2] Mortensen, A., Llorca, J., Metal Matrix Composites, Annu. Rev. Mater. Res., 40(1) 2010) 243–270.
[3] Deville, S., Ice-templating, freeze casting: Beyond materials processing, J. Mater. Res., 28(17) (2013) 2202–2219.
[4] Waschkies, T., Oberacker, R., Hoffmann, M. J., Control of lamellae spacing during freeze casting of ceramics using double-side cooling as a novel processing route, Journal of the American Ceramic Society, 92(1) (2009).
[5] Roy, S., Butz, B., Wanner, A., Damage evolution and domain-level anisotropy in metal/ceramic composites exhibiting lamellar microstructures, Acta Mater., 58(7) (2010) 2300–2312.
[6] Roy, S., Wanner, A., Metal/ceramic composites from freeze-cast ceramic preforms: Domain structure and elastic properties, Compos. Sci. Technol., 68(5) (2008) 1136–1143.
[7] Tsai, S. W., Strength Theories of Filamentary Structures, in Fundamental aspects of fiber reinforced plastic composites, R. T. Shwartz and H. S. Shwartz, Eds. New York: Wiley Interscience, (1968) 3–11.
[8] Deville, S., Freeze-casting of porous ceramics: A review of current achievements and issues, Adv. Eng. Mater., 10(3) (2008) 155–169.
[9] Hu, M., Yang, J., Cao, H., Evans, A., Mehrabian, R., The mechanical properties of Al alloys reinforced with continuous Al_2O_3 fibers, Acta Metall. Mater., 40(9) (1992) 2315–2326.